8948 *Biochemistry* **2009,** *48,* 8948–8957
DOI: 10.1021/bi9010072

BIOCHEMISTRY
including biophysical chemistry & molecular biology
Article

Exploring Damage Recognition Models in Prokaryotic Nucleotide Excision Repair with a Benzo[*a*]pyrene-Derived Lesion in UvrB[†]

Lei Jia,[‡,⊥] Konstantin Kropachev,[§] Shuang Ding,[‡] Bennett Van Houten,[∥,@] Nicholas E. Geacintov,[§] and Suse Broyde*[,‡,§]

[‡]*Department of Biology and* [§]*Department of Chemistry, New York University, 100 Washington Square East, Room 1009, New York, New York 10003, and* [∥]*Laboratory of Molecular Genetics, National Institute of Environmental Health Sciences, National Institutes of Health, 111 T. W. Alexander Drive, Research Triangle Park, North Carolina 27709* [⊥]*Present address: Pacific Biosciences Inc., 1505 Adams Dr., Menlo Park, CA 94025.* [@]*Present address: Department of Pharmacology and Chemical Biology, University of Pittsburgh, 5117 Centre Ave., Pittsburgh, PA 15232.*

Received June 15, 2009; Revised Manuscript Received August 10, 2009

ABSTRACT: The UvrB protein is a central unit for damage recognition in the prokaryotic nucleotide excision repair system, which excises bulky DNA lesions. We have utilized molecular modeling and MD simulations based on crystal structures, mutagenesis, and fluorescence data, to model the 10*R*-(+)-*cis*-*anti*-B[*a*]P-N^2-dG lesion, derived from the tumorigenic (+)-*anti*-B[*a*]PDE metabolite of benzo[*a*]pyrene, at different locations on the inner and outer strand in UvrB. Our results suggest that this lesion is accommodated on the inner strand where it might translocate through the tunnel created by the β-hairpin and UvrB domain 1B and ultimately could be housed in the pocket behind the β-hairpin prior to excision by UvrC. Lesions that vary in size and shape may be stopped at the gate to the tunnel, within the tunnel, or in the pocket when UvrC initiates excision. Common features of β-hairpin intrusion between the two DNA strands and nucleotide flipping manifested in structures of prokaryotic and eukaryotic NER lesion recognition proteins are consistent with common recognition mechanisms, based on lesion-induced local thermodynamic distortion/destabilization and nucleotide flipping.

Damage to DNA occurs continuously in living organisms, either endogenously through reactive oxygen species (ROS)[1] produced during normal metabolic processes or exogenously from sunlight, pollutants, dietary mutagens, and other factors (*1*). To preserve the DNA as the reliable storehouse for genetic information, repair mechanisms play a vital role in maintaining DNA integrity (*2*, *3*). Nucleotide excision repair (NER) is the predominant pathway for repair of bulky DNA lesions (*4*−*6*).

In prokaryotes, the dual incisions induced by the NER apparatus involve the UvrABC repair system. The UvrABC system consists of three proteins: UvrA, UvrB, and UvrC (*7*, *8*). The incision pathway is initiated when UvrA and UvrB form a heterotrimeric ($UvrA_2B$) (*9*) or heterotetrameric ($UvrA_2B_2$) (*10*) complex with the DNA lesion. This complex is believed to initially recognize the distortion/destabilization of the DNA duplex caused by bulky lesions. At this stage, the damaged DNA interacts primarily with the $UvrA_2$ units (*11*). A recently published crystal structure of UvrA identifies the UvrA dimerization interface that is regulated by ATP and suggests the location of the DNA and UvrB binding domains (*12*). After an ATP hydrolysis cycle, the damaged DNA moves to the binding domain of the UvrB unit and the $UvrA_2$ units leave (*7*). Recently, it has been shown that DNA wrapping around UvrB, mediated by UvrA, is an early recognition event (*13*). Thus, UvrB is the central component of the bacterial NER system that recruits the nuclease UvrC to the complex. Most recently, the crystal structure of the complex between the interaction domains of UvrA and UvrB was reported (*14*). A structural model for the full-length UvrA−UvrB assembly was constructed, and two models for lesion recognition involving these two enzymes were proposed: the recruitment and the handoff model. In the recruitment model, lesion recognition is exclusively achieved by UvrA, and UvrB binding occurs without lesion contact. In the handoff model, the damaged site is handed off to UvrB (*14*). The handoff model is consistent with earlier work suggesting that UvrB is directly involved in distinguishing damaged from undamaged DNA, and that it locates the position of the damage and guides the damaged DNA strand from the recognition to the repair stage (*15*). At the damaged site, the duplex DNA is separated by a UvrB β-hairpin protruding between the two strands; this generates an inner strand between itself and domain 1B (domains are defined in Figure 1A) of UvrB, and an outer strand on the exposed side (*15*). A change in the conformation of the UvrB−DNA complex triggers the recognition by the third component of the UvrABC system, UvrC. At this stage, the UvrB−DNA complex is in the preincision state, ready for processing by UvrC. In *Escherichia coli* UvrABC, UvrC carries out incisions at approximately the fifth phosphodiester

[†]This work was supported by the National Institutes of Health, National Cancer Institute Grants CA28038 to S.B. and CA099194 to N.E.G., and the NIEHS, NIH, Intramural Research Program to B.V.H. Partial support for computational infrastructure and systems management was also provided by Grant CA75449 to S.B. Computational support was provided in part by the National Science Foundation Partnerships for Advanced Computational Infrastructure.

*To whom correspondence should be addressed. Telephone: (212) 998-8231. Fax: (212) 995-4015. E-mail: broyde@nyu.edu.

[1]Abbreviations: ROS, reactive oxygen species; NER, nucleotide excision repair; (+)-*anti*-B[*a*]PDE, (+)-7*r*,8*t*-dihydrodiol-*t*9,10-epoxy-7,8,9,10-tetrahydrobenzo[*a*]pyrene; (+)-*cis*-B[*a*]P-N^2-dG, 10*R*-(+)-*cis*-*anti*-B[*a*]P-N^2-dG; SD, steepest descent; CG, conjugate gradient; rmsd, root-mean-square deviation; BER, base excision repair; CPD, cyclobutane pyrimidine photodimer; PDB, Protein Data Bank.

 Published on Web 08/14/2009

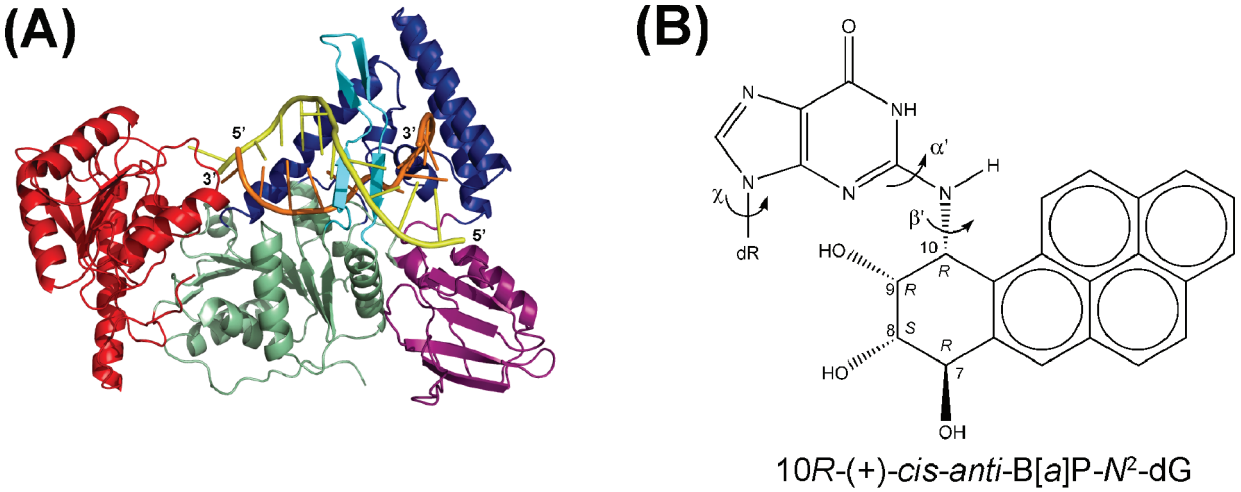

(C)

Model 1 (Lesion in the pocket)

Inner Strand	5′	C1	C2	A3	T4	C5	G6*	C7	T8	A9	C10	C11	3′
Outer Strand	3′	G22	G21	T20	A19	G18	C17	G16	A15	T14	G13	G12	5′

Model 2 (Lesion in the tunnel)

Inner Strand	5′	C1	A2	T3	C4	G5*	C6	T7	A8	C9	C10	G11	3′
Outer Strand	3′	G22	T21	A20	G19	C18	G17	A16	T15	G14	G13	C12	5′

Model 3 (Lesion at the gate)

Inner Strand	5′	A1	T2	C3	G4*	C5	T6	A7	C8	C9	G10	C11	3′
Outer Strand	3′	T22	A21	G20	C19	G18	A17	T16	G15	G14	C13	G12	5′

Model 4 (Lesion on the outer strand)

Inner Strand	5′	C1	G2	G3	T4	A5	G6	C7	G8	A9	T10	G11	3′
Outer Strand	3′	G22	C21	C20	A19	T18	C17	G16*	C15	T14	A13	C12	5′

FIGURE 1: (A) UvrB−DNA model. The UvrB−DNA complex model is shown as a cartoon. The domains of UvrB are color coded as follows: domain 1A (residues 1−151, 324−340, and 379−411), green; domain 1B (residues 252−323 and 341−378), blue; domain 2 (residues 151−251), purple; domain 3 (residues 412−593), red. The β-hairpin which belongs to domain 1A is colored cyan. The DNA inner strand (located between the protein and the β-hairpin) is colored orange, and the outer DNA strand is colored yellow. (B) Structure of the 10*R*-(+)-*cis*-*anti*-B[*a*]P-N^2-dG adduct. The absolute configurations of the four chiral atoms (C7, C8, C9, and C10) are indicated. Torsion angles are defined as follows: χ = O4′(dR)−C1′(dR)−N9−C4, α' = N1−C2−N^2−C10(B[*a*]P), β' = C2−N^2−C10(B[*a*]P)−C9(B[*a*]P) (dR is deoxyribose). (C) Base sequences and base numbering conventions of the four models considered. The B[*a*]P diol epoxide-modified guanine (G*) is indicated by the green background and is positioned on the inner strand in models 1, 2, and 3 and on the outer strand in model 4. The flipped-out bases in the initial models are colored yellow.

bond on the 3′ side and approximately the eighth bond on the 5′ side of the damaged base; the exact length of the excised oligonucleotide can depend on the nature of the adduct and the sequence context (*7*, *16*−*20*).

The intrinsic fluorescence of 2-aminopurine (2-AP) positioned on the damaged strand flanking a lesion on its 3′ side has been utilized to demonstrate that this base is flipped out of the duplex and is positioned in a hydrophobic region of the UvrB protein (*21*). Further fluorescence studies have recently shown that this flipped-out base helps stabilize the UvrB−DNA binding complex (*22*). In addition, studies with UvrB mutants have shown that stacking interactions occur between UvrB tyrosine residues and several flipped-out bases around the damaged base, including one on the damaged strand and one on the partner strand (*23*−*25*).

An X-ray crystallographic study (*26*) has revealed the structure of a *Bacillus caldotenax* UvrB complex with double-stranded DNA (part of a hairpin loop) containing a single-stranded 3′ end overhang and a fluorescein-derived lesion. While this structure did not have the lesion positioned in the recognition site, it provided essential information about the mode of DNA binding and the relevant amino acid residues in UvrB that are important for damage recognition. In this structure, three bases on the single-strand overhang behind the β-hairpin make multiple contacts with several amino acids, including Tyr92 and Tyr93, and one base is flipped out and stabilized by stacking over Phe249 (*26*). However, exactly where the lesion is positioned remains uncertain: the bulky fluorescein adduct is not positioned in close contact with the β-hairpin motif that is believed to contain the lesion recognition region; instead, it is adventitiously placed in the loop of the DNA hairpin, near the interface between domains 1A and 3 of UvrB. On the basis of the crystal structure and fluorescence data (*21*), a possible positioning of the damaged

base on the inner strand was suggested by Truglio *et al*. (*26*) to be just outside the tunnel created by the β-hairpin, with the last base pair of the duplex making strong contacts with Tyr96, and the next 3′ base flipped out into a "shape-complementary (planar) pocket" created in part by Phe249. The possible positioning of the lesion on the inner strand at the gate to the tunnel was also suggested from a crystal structure of UvrB containing a single-stranded dT 5mer oligonucleotide with a fluorescein adduct. In this case, two of the five dT residues were positioned behind the β-hairpin, and the large lesion was linked to a dT positioned at the β-hairpin/domain 1B interface; this structure suggested simple steric exclusion as inhibiting translocation of this very bulky lesion through the β-hairpin (*27*). Another position for the lesion would be inside the tunnel as suggested by Truglio *et al*. (*26*), who indicated that the damaged base at the tunnel gate would be the next one to be translocated behind the β-hairpin into the pocket created by Phe249. Finally, it is also possible that the damage may reside on the outer strand (*7*, *26*): a suggestion that this may occur stems from the observation that DNA photolyase bound to a pyrimidine dimer in the dark stimulated incision by the UvrABC system (*28*, *29*) which would indicate a modified outer strand for this case.

The objective of this work was to analyze possible lesion positioning mechanisms of the UvrB enzyme in complex with damaged DNA as in the handoff model (*14*), using molecular modeling and dynamics methods. We selected for investigation a bulky lesion derived from the reaction of the highly tumorigenic and mutagenic metabolically activated form of the environmental pollutant benzo[*a*]pyrene (*30*), (+)-7*r*,8*t*-dihydrodiol-*t*9,10-epoxy-7,8,9,10-tetrahydrobenzo[*a*]pyrene [(+)-*anti*-B[*a*]PDE], with the exocyclic amino group of guanine in double-stranded DNA. Reaction between guanine and (+)-*anti*-B[*a*]PDE produces two stereoisomeric adducts, the 10*S*-(+)-*trans*-*anti*-B[*a*]P-N^2-dG and 10*R*-(+)-*cis*-*anti*-B[*a*]P-N^2-dG adducts (*31*, *32*). While the 10*S*-(+)-*trans*-*anti*-B[*a*]P-N^2-dG stereoisomer is the predominant reaction product, the 10*R*-(+)-*cis*-*anti*-B[*a*]P-N^2-dG [(+)-*cis*-B[*a*]P-N^2-dG] stereoisomer is more efficiently incised by the *B. caldotenax*, *Thermotoga maritima*, and *E. coli* UvrABC system (*19*, *33*) and hence was selected for this study.

We built models of UvrB−DNA preincision complexes, based on available crystal structures of UvrB (*26*, *34*, *35*), and then explored four possible binding sites for positioning the lesion based on crystallographic data (*26*−*28*), fluorescence evidence (*21*), and mutation studies (*23*−*25*). Specifically, we considered [1] lesion placement on the inner strand in the UvrB shape-complementary (planar) pocket behind the β-hairpin; [2] lesion placement on the inner strand in the tunnel between the β-hairpin and domain 1B; [3] lesion placement on the inner strand at the gate before entering the tunnel; and [4] lesion placement on the outer strand in front of the β-hairpin. We conducted 5 ns molecular dynamics simulations and analyzed the resulting ensembles. Our results suggest that this lesion is housed on the inner strand where it might translocate through the tunnel between the β-hairpin and domain 1B and could finally be located in the hydrophobic pocket behind the β-hairpin prior to excision by UvrC. Differently sized and shaped lesions may be halted at the gate to the β-hairpin tunnel or become trapped in the tunnel prior to excision. The UvrB β-hairpin intrusion model bears a resemblance to the insertion of a hairpin between the two DNA strands at the lesion site by the yeast Rad4 NER protein, the orthologue of the human NER recognition factor XPC (*36*).

METHODS

Molecular Modeling of the Preincision State of the UvrB−DNA Adduct Complex. Since there is no crystal structure of a UvrB−DNA complex with any adducts at its binding site, we created a model, based on three crystal structures: a UvrB−DNA complex (*26*) (PDB entry 2FDC); a ternary complex containing UvrB, a polythymidine trinucleotide, and ADP (*34*) (PDB entry 2D7D); and a UvrB in the ATP-bound form (*35*) (PDB entry 1D9Z). The three UvrB crystal structures share considerable structural similarities. The 2FDC structure (chain B) from *Bca* was employed as the template structure since it is currently the only structure of a UvrB−DNA duplex complex containing the β-hairpin motif with the inner strand behind the hairpin. However, the outer strand stops before reaching the β-hairpin. Also, the ATP cofactor, needed for the preincision UvrB−DNA complex to bind UvrC (*7*), is missing. In addition, the adduct is not located near the β-hairpin region (*21*). Furthermore, eight residues (residues 477−484) are missing in the 2FDC structure, causing the secondary structure from residue 485 to 489 to be misfolded as compared to the relatively complete structure of 2D7D. Note that UvrB C-terminal domain 4 is missing in most structures (only partially resolved in crystal structure 2D7D). UvrB domain 4 is an autoinhibitory domain involved in UvrC binding and UvrB dimerization and inhibits DNA binding and ATP hydrolysis (*10*, *37*, *38*). Thus, we could not model domain 4 in our work. Further molecular modeling was needed to build the preincision UvrB−DNA complex, as described below.

The sequence of the 11mer double-stranded DNA investigated was selected because it has been used in previous experimental UvrABC DNA repair studies (Figure 1C) (*19*, *33*). The 2FDC crystal structure contains 3 bp of double-stranded DNA with a 2-base 3′ overhang, corresponding to 5′-A3-T4-C5-G6-C7-3′/3′-T20-A19-G18-5′ in Figure 1C, model 1. We elongated the DNA duplex by modeling two nucleotides on the outer strand, G16 and C17, to wrap around the β-hairpin and then added four more base pairs (5′-T8-A9-C10-C11-3′/3′-A15-T14-G13-G12-5′) beyond the two separated strands emanating from the β-hairpin. C17 on the outer strand was modeled to be flipped out on the basis of the fluorescence data (*21*). The G16 on the outer strand was also modeled to be flipped out, stacking with Tyr95, based on mutation studies (*24*, *25*). We then added one base pair, T8·A15, which neighbors the C7·G16 base pair on the right side of the β-hairpin (Figure 2). Bases T8 and A15 on the inner and outer strands, respectively, were modeled to be base paired by manually adjusting the DNA backbone and glycosidic torsion angles. The three remaining base pairs were added using the NMR solution structure (*39*) of the 11mer duplex containing the B[*a*]P adduct, utilizing the last three base pairs 3′ to the lesion.

The ATP cofactor with a coordinated Mg^{2+} was modeled in the ATP binding site of 2FDC from crystal structure 1D9Z by superimposing residues 11−46 of 2FDC and 10−45 of 1D9Z (Figure S1 of the Supporting Information). These residues form the ATP binding pocket. To model the eight missing residues, we superimposed residues 420−460 of 2FDC on residues 418−458 of 2D7D and then modeled residues 477−489 from 2D7D onto 2FDC (Figure S1).

The B[*a*]P base adduct coordinates (Figure 1B) were obtained from the NMR solution structure (*40*) and modeled into the hydrophobic pocket suggested by Truglio *et al*. (*26*) by covalently linking the inner strand guanine (G6) N^2 atom to the B[*a*]P C10 atom. To be housed in the pocket, the glycosidic conformation

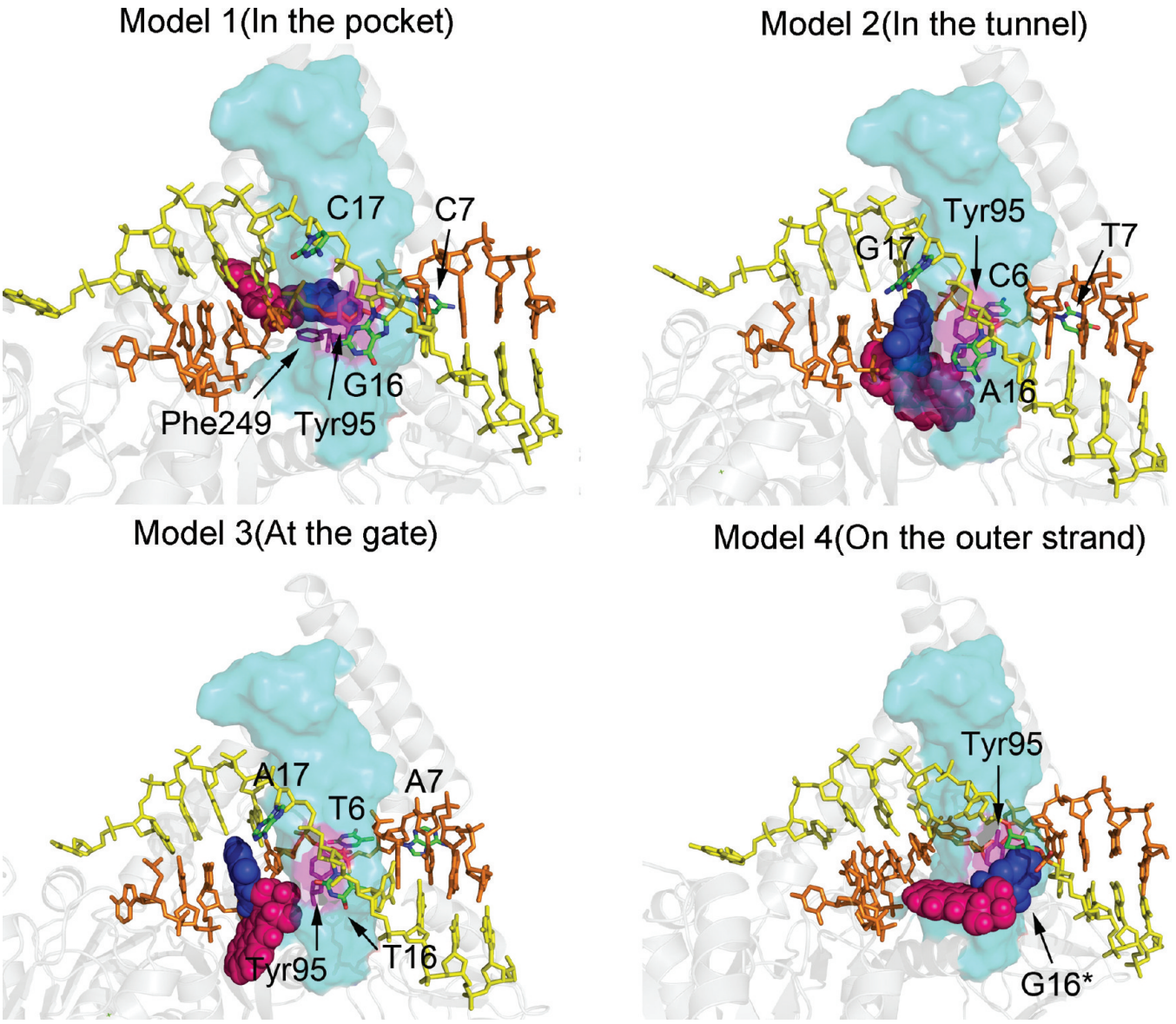

FIGURE 2: Initial models of the four UvrB−DNA complexes. Model 1 has the adduct positioned in the UvrB pocket. Model 2 has the adduct positioned in the tunnel between the β-hairpin and domain 1B. Model 3 has the adduct positioned at the gate before entering the tunnel. Model 4 has the adduct positioned on the DNA outer strand. The UvrB protein is rendered as a cartoon, while the DNA is rendered as a stick. The β-hairpin is rendered as a cyan transparent surface. The B[*a*]P-dG is rendered as a CPK model with G6* colored blue and B[*a*]P colored magenta. The DNA inner strand is colored orange and the outer strand yellow. The flipped-out bases and Tyr95 are labeled; these bases are colored by atom, and Tyr95 is colored magenta. A stereoview is given in Figure S6 of the Supporting Information.

has to be in the *syn* conformation. These strategies were utilized to generate model 1 (Figure 2).

We also modeled the B[*a*]P adduct in positions G5 (model 2) and G4 (model 3) to investigate the translocation of the adduct within the UvrB complex (Figure 2). Models 2 and 3 were constructed using model 1 as a basis, but with the appropriate modification of the adduct site relative to the protein (Figure 1C). At both positions G4 and G5, the guanine must be in the *syn* conformation to minimize collisions with protein residues. At position G5, the *syn* guanine is still stacked with Tyr96 of UvrB, consistent with observations from both crystallography (*26*) and experiments with UvrB mutants which showed that binding to DNA was abolished when Tyr96 was mutated to alanine (*7*, *24*, *41*).

In addition, we modeled the adduct on the outer strand utilizing the sequence shown in Figure 1C to produce model 4. The B[*a*]P adduct was linked to the G16 base; the latter was modeled in a stacked conformation with Tyr95, as observed by Moolenaar *et al.* (*24*) and Zou *et al.* (*25*). To stack with Tyr95 and position the adduct without collisions, the G16 must be in the *syn* conformation (Figure 2 and Table S1).

Initial models were constructed to have minimal steric collisions by adjusting the (+)-*cis*-B[*a*]P-N^2-dG torsion angles χ, α', and β' (Figure 1B) to locate the optimal positions. We also made an effort to visually optimize favorable interactions between the damaged base and the enzyme, such as hydrophobic and electrostatic interactions. All χ, α', and β' torsions for the models are listed in Table S1. A total of four models were created. Hydrogen atoms were added with the LEaP module in AMBER 8.0 (*42*). Each complex was then energy-minimized with implicit solvent (dielectric constant of 4.0r, while r is the distance between two atoms) for 400 steps of steepest descent (SD) followed by 600 steps of conjugate gradient (CG) minimization using the SANDER module of AMBER 8.0 (*42*).

Force Field. Computations were conducted with the AMBER 8.0 suite of programs (*42*), the Cornell *et al.* force field (*43*), and the PARM99 parameter set (*44*). The force field for the (+)-*cis*-B[*a*]P-N^2-dG adduct was parametrized in a manner consistent with the rest of the AMBER force field: partial charges were computed as described previously (*45*), and atom types were defined on the basis of the PARM99 and GAFF (*46*) parameter sets. Missing parameters were assigned by analogy with chemically similar atom types already present in the force field. All of the added force field parameters, atom types, and topology assignments are listed in Tables S2−S4.

Molecular Dynamics Protocol. Full details of the MD protocol are given as Supporting Information.

Stability of the Molecular Dynamics Simulation. Plots of the root-mean-square deviations (rmsds) of the current relative to the starting structure as a function of time are shown in Figure S2. The structures generally fluctuate in a stable manner after 2 ns, and our analyses were confined to the 2.0−5.0 ns time frame. We selected one best representative structure from each ensemble for graphic illustration. To pick the best representative structure, we extracted 100 structures at 30 ps intervals from the 2−5 ns time frame for each model. Each extracted structure was superimposed on the 99 remaining structures, and the rmsds were computed and summed. The structure with the smallest sum rmsd was selected as the most representative structure (Table S6). This procedure essentially follows the philosophy in MoilView (*47*), which could not be utilized because of the size of our system.

Structural Analyses. Snapshots of the structures during the simulations and the average structures with solvent and counterions removed were obtained with the PTRAJ module of the AMBER 8.0 suite (*42*). PTRAJ was also employed to determine the time dependence of the rmsd, and of torsion angles α', β', and χ. These are given in Figure S3, which shows that these torsions occupy limited domains as previously delineated by molecular mechanical calculations (*48*). Detailed hydrogen bonding analyses were conducted with the CARNAL module of the AMBER 7.0 suite (*49*).

INSIGHT II and Discovery Studio from Accelrys, Inc., and PyMOL (*50*) from DeLano Scientific LLC were employed for visualization and model building. Computations were conducted on our own cluster of Silicon Graphics Origin and Altix high-performance computers.

RESULTS

The objective of this work was to systematically explore different structural hypotheses for the possible binding sites of the lesion in UvrB. Is the adduct positioned within the UvrB protein on the inner strand or the outer strand? If on the inner strand, is the lesion blocked at the UvrB β-hairpin steric gate or can it translocate through the tunnel behind the β-hairpin? For these purposes, we constructed four models, all based on available experimental data, of complexes containing UvrB and double-stranded DNA with the (+)-*cis*-B[*a*]P-N^2-dG adduct either on the inner or on the outer strand (see Methods). The exact sequences and the base numbering schemes that were used in modeling the different translocation steps are shown in Figure 1C. The lesion was positioned on the inner strand in the pocket behind the β-hairpin (model 1), in the "tunnel" between the β-hairpin and domain 1B (model 2), at the entrance to the tunnel (model 3), and on the outer strand contacting the β-hairpin (model 4). Molecular dynamics simulations were performed in each case. The MD trajectories were evaluated, and the lesion positioning and the possibility of lesion translocation through the β-hairpin of the UvrB protein were examined.

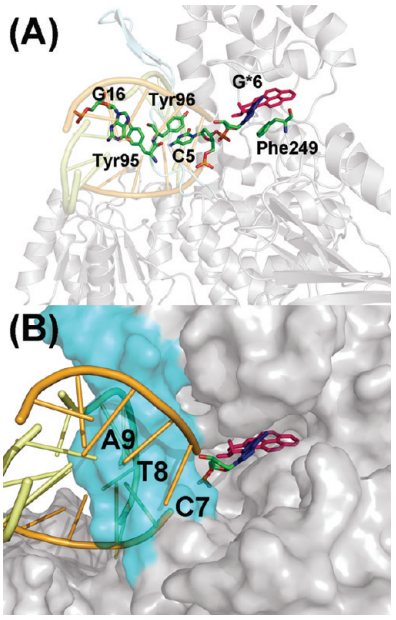

FIGURE 3: Model 1 of the adduct in the pocket of UvrB. The B[*a*]P-dG adduct is shown as a stick with G6* colored blue and B[*a*]P colored magenta. Hydrogen atoms have been omitted for the sake of clarity. (A) The stacking interactions that stabilize the binding of the DNA molecules to UvrB are shown. The residues involved in stacking interactions are shown in the stick model with color coding by atom. (B) Accommodation of the B[*a*]P residue in the pocket behind the β-hairpin (the latter colored cyan). The UvrB protein is shown in the surface model mode. The best representative structure is shown. A stereoview is given in Figure S7.

Structures of the UvrB−DNA Preincision Complex. The initial model of the UvrB−DNA preincision complex was based mainly on crystal structure 2FDC (*26*) of the *Bca* UvrB protein containing the modified DNA sequence context 5′-...CCATCG*C-TACC..., with G* designating the modified guanine. The complex in the crystal structure has a DNA single-strand region as well as a pocket with a flat floor motif, both located behind the β-hairpin; this pocket appears to be capable of accommodating the DNA adduct when the damaged site is located on the inner DNA strand between the hairpin and surface of the UvrB protein (*26*). The B[*a*]P residue was positioned in this pocket (see Methods) (model 1 of the preincision complex) with minimal close contacts (Table S1). To study the feasibility of translocation of the adduct through the β-hairpin, we also positioned the lesion at G5 and G4 on the inner strand (models 2 and 3, respectively). In all models, the sequence context in which the (+)-*cis*-B[*a*]P-N^2-dG adduct is embedded is constant, and only the position of the adduct is different.

The feasibility of positioning the lesion on the outer DNA strand of the DNA duplex was investigated by modeling the lesion at G16 (Figure 1C) where the modified guanine is stacked with Tyr95 (model 4), as suggested by experiments with mutants (*24*, *25*). In this case, G6 is positioned in the pocket.

Accommodation of the Lesion in the Pocket behind the β-Hairpin. The bulky and hydrophobic B[*a*]P residue can be positioned in the spacious pocket located behind the β-hairpin, when the glycosidic bond of the modified guanine is in the *syn* conformation (model 1). This lesion-containing pocket is surrounded by the following residues (within 5 Å of any B[*a*]P atom): Tyr146, Gly147, Leu148, Gly149, Asn308, Ser310, Arg311,

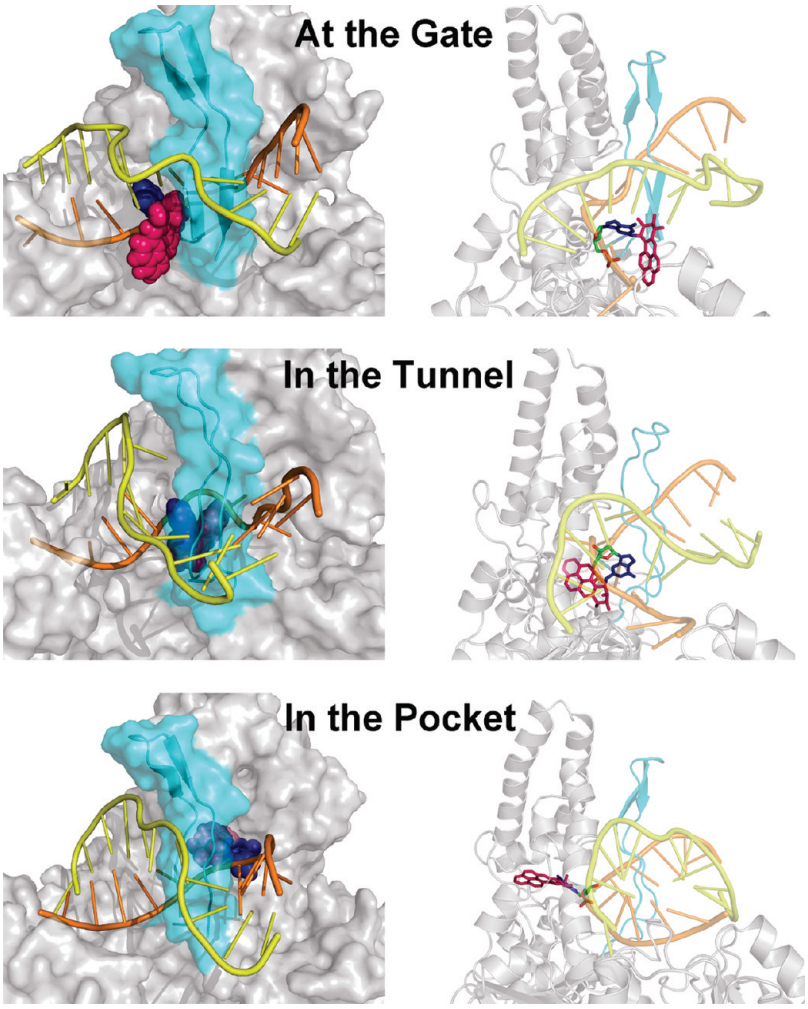

FIGURE 4: Possible translocation mechanisms illustrated for the adduct in terms of models 3, 2, and 1 (top to bottom, respectively). The left-hand panels show front views of the protein. The β-hairpin is colored cyan and is semitransparent so that the adduct behind the hairpin can be discerned. The adduct is in the CPK model. G6* is colored blue and B[*a*]P magenta. The DNA inner strand is colored orange and the outer strand yellow. The right-hand panels show views of the DNA−UvrB complex looking into the tunnel from the left side. UvrB is shown as a cartoon. The adduct is shown as a stick model. Hydrogen atoms have been omitted for the sake of clarity. The color code is the same as in the left-hand panels. These images suggest that the B[*a*]P lesion can be translocated past the β-hairpin; while the upper part of the β-hairpin remains in contact with domain 1B, the bottom part moves away to enlarge the tunnel. The best representative structures are shown. Stereoviews are given in Figures S8 and S9.

Thr312, Ser320, Pro322, Tyr323, Asp354, Lys358, Asp373, Asn374, Arg375, and Pro376. The interactions between the adduct and the protein in the pocket are mainly hydrophobic. At the modified site, the damaged guanine is flipped out of the DNA. The simulation results suggest that the positions of the modified guanine and several of its neighboring bases are stabilized by stacking interactions with several amino acid residues (Figure 3A). Specifically, a stacking interaction between the modified guanine residue and Phe249 stabilizes the flipped-out base. It should be noted that there is an analogous stacking interaction between Phe249 and an undamaged cytosine in the crystal structure (*26*). Furthermore, Tyr96 stacks with C5 which is on the 5′ side of the modified guanine, which retains a buckled base pair with G18; this stacking interaction was also present in the starting model and remained stable throughout the simulations. In addition, on the outer strand, base G16, which is the partner base of C7, is stacked with Tyr95 in the β-hairpin, and this interaction is also maintained throughout the simulation (Figure 3A).

Possibilities for Lesion Translocation behind the UvrB β-Hairpin. To investigate the possibility of translocation of the bulky lesion positioned on the inner DNA strand behind the β-hairpin of UvrB, we modeled the B[*a*]P adduct at three consecutive positions on this trajectory. These include the G6 position of the adduct with the adduct in the pocket as described above (model 1), or the G5 position (model 2) and the G4 position (model 3) (Figure 1C). The hypothesis here is that the bulky adduct on the inner strand needs to translocate through the β-hairpin to achieve binding in the pocket as shown in model 1 (see the movie in the Supporting Information). At the G4 position, the adduct is close to the β-hairpin where the aromatic rings are partly solvent exposed; however, the lesion does not enter the tunnel between the β-hairpin and domain 1B of UvrB (Figure 4). At the G5 position, our models reveal that the adduct can reside behind the β-hairpin and become stably accommodated within the tunnel. It is not necessary for the β-hairpin to completely separate from domain 1B (Figure 4) to allow for the translocation of bulky adducts that are comparable in size to the (+)-*cis*-B[*a*]P-N^2-dG adduct considered here. The upper part of the β-hairpin motif is still in contact with the UvrB domain 1B. However, the bottom of the β-hairpin changes conformation from a well-organized β-sheet to a loop. This enables the root of the β-hairpin to move away from domain 1B, which enlarges the tunnel to allow the lesion to pass (Figure 4). When the adduct is at the G6 position in the

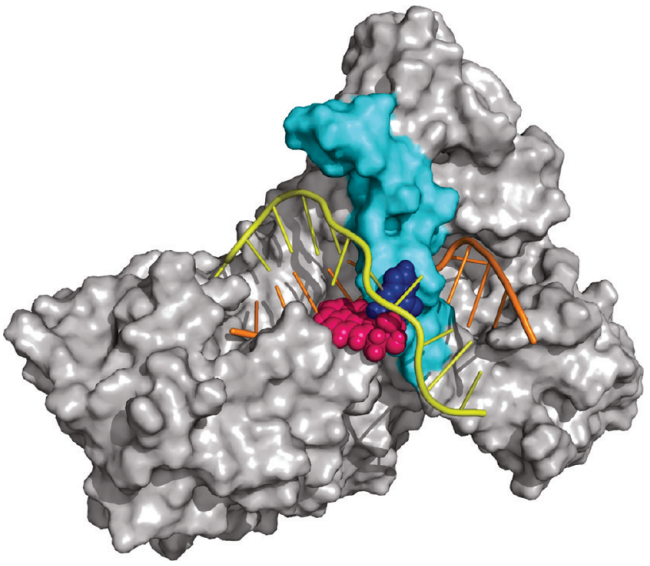

FIGURE 5: Model 4 of the adduct positioned in the DNA outer strand in the UvrB complex. The UvrB protein is shown as a surface model. The β-hairpin is colored cyan. The damaged DNA is shown as a cartoon. The DNA inner strand is colored orange and the outer strand yellow. The largely solvent-exposed B[*a*]P-dG adduct is shown as a CPK model with G6* colored blue and B[*a*]P colored magenta. The best representative structure is shown. A stereoview is given in Figure S10.

Table 1: Flipping and Stacking Properties of the Bases in Representative Structures of Each Model[a]

	model 1 (pocket)	model 2 (tunnel)	model 3 (gate)	model 4 (outer)
base 6	F/S	F/S	F/S	F/S
base 7	N	F	F	F
base 16	S	N	N	S
base 17	F	N	N	F

[a]F denotes flipped-out bases. S denotes a stacking interaction: base 6 stacks with Phe249, and base 16 stacks with Tyr95. N designates no flipping or stacking with amino acid residues. Figure S4 shows these flipping and stacking properties for all the models.

pocket, the lesion may pass through the step that involves model 2 in which it is in the tunnel (Figure 4).

Accommodation of the Lesion on the Outer Strand: Dynamic and Solvent-Exposed. When the B[*a*]P adduct is on the outer strand in model 4, the hydrophobic adduct fits nicely into a shallow cavity of the UvrB protein between the β-hairpin and domain 1A (Figures 5 and S10). The system is more dynamic than in the other models as shown by the rmsd plots of the damaged DNA (Figure S2). While there is substantial solvent exposure of the B[*a*]P aromatic rings, they appear to be minimizing this property by their neat fit into the UvrB cavity with further shielding by flipped-out base C17. Nonetheless, the outer strand model has the greatest solvent exposure for the damaged nucleotide. We computed the solvent-exposed surface area for the damaged nucleotide in the most representative structure in each of our models using Discovery Studio and obtained the following values: model 1 (pocket), 63 Å^2; model 2 (tunnel), 36 Å^2; model 3 (gate), 151 Å^2; and model 4 (outer strand), 269 Å^2.

Flipped-Out Bases in Our Models. Our initial models contained flipped-out bases, consistent with crystallographic, mutation, and fluorescence data (*21*, *24*−*26*, *41*). Specifically, in the pocket model (model 1), the unmodified base G16 in the complementary strand is flipped out and stacked with Tyr95. Base C17, also in the complementary strand but opposite the lesion (Figure 1C), is also flipped out of the duplex to wrap the outer strand around the β-hairpin. B[*a*]P-modified base G6* is flipped into the pocket and is stacked with Phe249. C7 on the 3′ side of damaged base G6* is also flipped out. In models 2 and 3, the bases in the analogous positions (yellow-colored bases in Figure 1B) are flipped out. In model 4, B[*a*]P-modified base G16 is flipped out and also stacks with Tyr95. However, the most representative structures following our MD simulations showed variable flipping patterns as summarized in Table 1 and shown in Figure S4. For example, in model 1, the C7 which is 3′ to the lesion rotated from its initial flipped out position, so that it was mainly stacked with T8 after simulation for 1 ns (Figure S5).

DISCUSSION

Inner and Outer Strand Models: The (+)-cis-B[a]P-N^2-dG Adduct Can Be Accommodated in UvrB on the Inner Strand and Can Be Housed in a Pocket behind the β-Hairpin. Since a crystal structure of a UvrB−DNA complex is available which reveals that the DNA duplex is partially separated by the β-hairpin protruding into the double helix, the question of whether the damaged base is located on the inner or outer DNA strand, relative to the hairpin, has remained a matter of debate (*26*). In a repair study, DNA photolyase bound to a pyrimidine photodimer was shown to stimulate incision by the UvrABC repair system (*29*). DNA photolyases catalyze the cleavage of the cyclobutane ring, using blue or near-UV light as the energy source (*51*, *52*). A crystal structure of the photolyase−DNA complex (*28*) showed that the damaged pyrimidines were flipped out into the photolyase pocket. These observations suggest that in this special case, the UvrAB complex recognizes DNA photolyase bound to the pyrimidine dimer, which is apparently located on the outer strand of the UvrB−DNA complex to avoid the steric interference of the two repair systems (*26*). Our model 4 shows that if the damaged base is on the outer strand, the lesion as well as its 3′ flanking neighbor base would both be exposed to the solvent (Figures 5 and S10), although the B[*a*]P ring system is accommodated in a cavity between the β-hairpin and domain 1A. This model seems to be in disagreement with fluorescence studies (*21*) which suggested that the base flanking a cholesterol residue-modified lesion on the 3′ side is flipped into a hydrophobic cavity of the UvrB protein. However, in our model 4, C17 is solvent-exposed (Figure 5). In addition, for efficient UvrC incision to occur, a base on the unmodified strand must be flipped out and interact with Tyr95 (*21*, *22*). It was suggested that this base is the 5′ nearest neighbor to the partner base in the complementary strand opposite the lesion. However, G6 in model 4 is flipped out but stacked with Phe249 (Figure S4). These considerations suggest that the damaged base is positioned on the inner strand.

The crystal structures of the UvrB−DNA complex provide further insights into the location of the damaged base. The structure used as our modeling template suggests the existence of a binding pocket behind the β-hairpin which could be a location where the modified base can be accommodated (*26*). However, the structure of UvrB bound to a fluorescein-adducted DNA duplex suggested a "steric gate" model of the UvrB protein for this much larger adduct (*26*, *27*). In this model, there is a narrow tunnel between the β-hairpin and UvrB domain 1B [also shown in our model 3 (Figure 4)] which accommodates the

undamaged DNA single strand; however, a large lesion such as fluorescein with its long and flexible linkage to the modified base cannot pass through the tunnel. Hence, translocation is blocked, and the binding of UvrC and the subsequent incisions would be triggered by this blocked translocation. The steric gate model can be supported only if the adduct is located on the inner strand but is stopped before entering the tunnel behind the β-hairpin.

It is possible that the location of the damaged base in the DNA−UvrB complex, i.e., before UvrC is recruited, depends on the nature of the lesion and the specific recognition mechanism. For example, while the hydrophobic pocket behind the β-hairpin appears to be a plausible site for accommodating the hydrophobic (+)-*cis*-B[*a*]P-N^2-dG adduct, a hydrophilic lesion likely would not enter this pocket; one could speculate that it might remain in the tunnel if it were small enough to enter it. In the case of UvrABC-mediated repair of cyclobutane pyrimidine dimer bound by photolyase, the cyclobutane pyrimidine ring would have to be rotated outward or could possibly be located on the outer strand, to accommodate bound DNA photolyase. However, this would require UvrB to engage the nondamaged strand behind the hairpin. Perhaps, if the stoichiometry of UvrA and UvrB is two molecules of each as reported by Goosen and co-workers (*10*, *53*), one of the UvrB's could engage either strand once a helical perturbation is first sensed by UvrA. However, in the case of bulky adducts, such as cholesterol, fluorescein, menthol, and benzo[*a*]pyrene-derived adducts, which require that UvrC be utilized for incising more than 10 bp around the damaged site, the positioning of hydrophobic adducts on the inner strand appears to be favored, as suggested by the crystal structures (*26*, *34*, *35*), fluorescence experiments (*21*, *22*), and our models. Current knowledge of the repair mechanisms (*7*) and our models suggests that UvrB acts as a gauge to accurately recognize the location of the damaged base; the UvrC then binds to the UvrB−DNA complex to specifically incise the damaged strand at defined sites on the 3′ and 5′ sides of the damaged base. The UvrC endonuclease does not necessarily need to interact directly with the adduct to perform the incisions. A recently published crystal structure of the C-terminal half of UvrC revealed a likely binding mode of this enzyme with DNA, via a positively charged patch on the enzyme's surface (*54*). The full UvrB−UvrC interaction mechanism will undoubtedly become clearer as crystal structures of such complexes become available.

DNA−protein cross-links are also subject to repair by the UvrABC system if the protein is less than ∼12−14 kDa in size and also may be repaired by human NER (*55*). In our models, such unusually bulky lesions would need to be situated either at the steric gate (model 3) or on the outer strand (model 4).

β-Hairpin "Breathing" May Facilitate Lesion Translocation Behind It. One important feature of the UvrB protein is its ability to partially separate the damaged DNA duplex into its separate strands and locate the lesion by short translocations of the damaged DNA strand through the β-hairpin motif (*26*, *27*, *35*). To investigate translocation, we built three models to simulate the trajectory of the adducted DNA translocating through the β-hairpin in three consecutive steps. Model 3 shows the adduct positioned at the gate of the tunnel between the β-hairpin and domain 1B. Model 2 shows the adducted DNA translocated one base further in the 3′ direction of the damaged strand, with the B[*a*]P-modified base positioned in a location between the β-hairpin and domain 1B. Model 1, the pocket model, shows the DNA translocated one additional base step and the adduct has passed through the tunnel.

Model 2 reveals that the β-hairpin does not need to be completely separated from domain 1B to allow the damaged DNA with an adduct the size of the (+)-*cis*-B[*a*]P-N^2-dG adduct to translocate through the narrow tunnel. The bottom part of the β-hairpin changes its conformation to accommodate the bulky adduct, but the top is still in strong contact with domain 1B. On the other hand, a padlock model has been proposed (*7*, *15*), which suggests that the β-hairpin can separate from domain 1B to insert itself between the double strands of the damaged DNA, so that one strand is clamped between the β-hairpin and domain 1B. This separation would be required at the time of initial binding and separation of the damaged DNA duplex, at least for the case of closed circular DNA. The padlock model does not require translocation through the hairpin, although it may still occur after one DNA strand is clamped by the β-hairpin. The flexibility of the β-hairpin, seen in our simulations, suggests that the extent of hairpin breathing could vary, depending on the lesion shape and size, and that the hairpin could open as in the padlock model by separating from domain 1B if necessary. In the most extreme case, the lesion may be completely blocked at the tunnel entrance as in the steric gate model (*27*). A recent fluorescence study suggests the possibility that the nature of the lesion determines how far the damaged strand can translocate behind the β-hairpin (*22*). A cholesterol lesion linked directly to the DNA backbone is suggested to be translocated further behind the β-hairpin as compared to a menthol lesion which is directly linked to a base.

Hindered lesion translocation in UvrB may provide insights into the observations of Zou *et al*. (*19*), which show that in the case of the (+)-*cis*-B[*a*]P-N^2-dG lesion, 3′ incision occurs at the fifth, sixth, and seventh phosphates 3′ to the lesion, with the extent of incisions decreasing in the following order: fifth phosphate > sixth phosphate > seventh phosphate. This was also observed for DNA photoproducts in different sequence contexts (*17*). These three different incision modes, producing fragments of increasing length, might be explained by our three models: the pocket model, the tunnel model, and the gate model; together, these models might explain incisions at the fifth, sixth, and seventh phosphates on the 3′-side of the lesion, respectively. If the UvrC dual incision is facilitated by translocation stalling (*7*), the nonuniform probabilities of 3′ incisions at the phosphodiester sites could result: the relative incision rate at the seventh phosphate would be lowest when the lesion reaches the gate, suggesting that the adduct is stalled at this position for the shortest time. A further translocation would place the lesion within the tunnel where it may reside for a longer time, thus increasing the probability of incisions at the sixth phosphate. Finally, the lesion is stalled in the pocket, thus leading to the highest cleavage probability at the fifth phosphate. This hypothesis suggests a dynamic aspect of the dual incision mechanism that may depend on the size, shape, and conformation of the lesion (*19*).

Flipping Out of Bases and Intrusion of the β-Hairpin into the Double Helix. The 2-AP studies by Malta *et al*. (*21*) showed that several bases around the damaged site, including the base immediately adjacent to the lesion on the 3′ side, as well as its partner base on the complementary strand are flipped out of the DNA duplex. Using two different lesions, namely, a cholesterol lesion linked on the DNA backbone and a menthol-modified thymine, a more recent fluorescence study suggested that the specific position of the flipped base on the 3′ side of the lesion is dependent on the type of lesion (*18*). However, flipping of the nucleotide on the undamaged strand was shown to be

independent of lesion type, and both flipped bases are protected from solvent (*22*). Fluorescence measurements and experiments with mutants show that Tyr95 and Phe249 stack with the flipped-out bases on the damaged and partner strands (*21*, *24*, *25*, *41*). Our modeling studies are consistent with the possibility that the type of lesion determines which specific base on the 3′ side of the lesion is flipped, since, as detailed in Results, flipping patterns differ in the different models (Table 1).

A flip-out mechanism appears to be common to different DNA repair pathways and is well-established in the base excision repair (BER) pathway (*56*, *57*). In the NER pathway, a helix opening mechanism (*58*) that is likely to be accompanied by base flipping (*59*) seems to be important for lesion recognition and subsequent incisions. The crystal structure of the yeast Rad4 NER protein, the orthologue of human NER recognition factor XPC, shows that the partners of the cyclobutane pyrimidine photodimer (CPD) damage are flipped out (*36*). The extrusion of a base out of the duplex originates from local duplex distortion/destabilization by the lesion which facilitates intrusion of a β-hairpin between the strands at the lesion site. Thus, the prokaryotic (*26*) and eukaryotic (*36*) NER lesion recognition mechanisms share common structural features such as base flipping and β-hairpin intrusion between the strands of the DNA duplex at the lesion site.

CONCLUSION

We have utilized molecular modeling and molecular dynamics simulations evaluating all available experimental data to explore lesion housing and lesion translocation in UvrB. Our results suggest that the (+)-*cis*-B[*a*]P-N^2-dG lesion is located on the DNA strand behind the UvrB β-hairpin. It might pass through a tunnel formed by the β-hairpin and domain 1B and be housed in a pocket behind the β-hairpin. The undamaged DNA strand is on the outside of the tunnel. Overall, our models suggest that lesion size and shape would govern possibilities for traversing the tunnel or remaining jammed in front of it prior to excision by UvrC, possibly explaining differently sized excision products. Additionally, our results suggest unifying insights concerning the functioning of the prokaryotic UvrB and the yeast Rad4 ortholog of the human XPC protein (*36*). Specifically, both utilize the β-hairpin motif to intrude between the two strands of the damaged double helix and base flipping, manifesting common recognition features involving local thermodynamic destabilization with base extrusion (*60*). Interestingly, the UV DDB1−DDB2 damage recognition complex also utilizes hairpin intrusion and lesion extrusion for damage recognition (*61*).

ACKNOWLEDGMENT

The content is solely the responsibility of the authors and does not necessarily represent the official views of the National Cancer Institute or the National Institutes of Health.

SUPPORTING INFORMATION AVAILABLE

The molecular dynamics protocol and a translocation movie are provided. Figure S1 shows the superimposition of the ATP binding site when modeling the ATP from 1D9Z into 2FDC, and the superimposition of protein residues 420−460 of 2FDC onto residues 418−458 of 2D7D to model a missing loop from 2D7D to 2FDC. Figure S2 shows plots of the all-atom rmsd of the current relative to the starting structure as a function of time for the whole UvrB−DNA complex, and for just the damaged and undamaged DNA strands. Figure S3 shows plots of the torsion angles χ, α', and β' for all complex models in the selected time frames for analysis. Figure S4 shows the flipping and stacking properties of the bases in representative structures of each model. Figure S5 shows the C7 base in the flipped-out and flipped-in position of model 1. Figures S6−S10 show stereoviews of Figures 2−5. Table S1 gives glycosidic torsion angle χ values in the initial models for MD simulations. Table S2 gives AMBER atom type, connection type, and partial charge assignments for the (+)-*cis*-B[*a*]P-N^2-dG adduct. Table S3 gives AMBER atom type, connection type, and partial charge assignments for ATP. Table S4 gives AMBER atom type, connection type, and partial charge assignments for Mg^{2+}. Table S5 gives box sizes and numbers of waters and counterions in the MD simulation initial models. This material is available free of charge via the Internet at http://pubs.acs.org.

REFERENCES

1. Lindahl, T. (1993) Instability and decay of the primary structure of DNA. *Nature 362*, 709–715.
2. Hoeijmakers, J. H. (2001) Genome maintenance mechanisms for preventing cancer. *Nature 411*, 366–374.
3. Lindahl, T., and Wood, R. D. (1999) Quality control by DNA repair. *Science 286*, 1897–1905.
4. de Laat, W. L., Jaspers, N. G., and Hoeijmakers, J. H. (1999) Molecular mechanism of nucleotide excision repair. *Genes Dev. 13*, 768–785.
5. Wood, R. D. (1997) Nucleotide excision repair in mammalian cells. *J. Biol. Chem. 272*, 23465–23468.
6. Leibeling, D., Laspe, P., and Emmert, S. (2006) Nucleotide excision repair and cancer. *J. Mol. Histol. 37*, 225–238.
7. Truglio, J. J., Croteau, D. L., Van Houten, B., and Kisker, C. (2006) Prokaryotic nucleotide excision repair: The UvrABC system. *Chem. Rev. 106*, 233–252.
8. Hoeijmakers, J. H. (1991) How relevant is the *Escherichia coli* UvrABC model for excision repair in eukaryotes? *J. Cell Sci. 100* (Part 4), 687–691.
9. Orren, D. K., and Sancar, A. (1989) The (A)BC excinuclease of *Escherichia coli* has only the UvrB and UvrC subunits in the incision complex. *Proc. Natl. Acad. Sci. U.S.A. 86*, 5237–5241.
10. Verhoeven, E. E., Wyman, C., Moolenaar, G. F., and Goosen, N. (2002) The presence of two UvrB subunits in the UvrAB complex ensures damage detection in both DNA strands. *EMBO J. 21*, 4196–4205.
11. DellaVecchia, M. J., Croteau, D. L., Skorvaga, M., Dezhurov, S. V., Lavrik, O. I., and Van Houten, B. (2004) Analyzing the handoff of DNA from UvrA to UvrB utilizing DNA-protein photoaffinity labeling. *J. Biol. Chem. 279*, 45245–45256.
12. Pakotiprapha, D., Inuzuka, Y., Bowman, B. R., Moolenaar, G. F., Goosen, N., Jeruzalmi, D., and Verdine, G. L. (2007) Crystal Structure of *Bacillus stearothermophilus* UvrA Provides Insight into ATP-Modulated Dimerization, UvrB Interaction, and DNA Binding. *Mol. Cell 29*, 122–133.
13. Wang, H., Lu, M., Tang, M. S., Van Houten, B., Ross, J. B., Weinfeld, M., and Le, X. C. (2009) DNA wrapping is required for DNA damage recognition in the *Escherichia coli* DNA nucleotide excision repair pathway. *Proc. Natl. Acad. Sci. U.S.A. 106*, 12849–12854.
14. Pakotiprapha, D., Liu, Y., Verdine, G. L., and Jeruzalmi, D. (2009) A structural model for the damage sensing complex in bacterial nucleotide excision repair. *J. Biol. Chem. 284*, 12837–12844.
15. Theis, K., Skorvaga, M., Machius, M., Nakagawa, N., Van Houten, B., and Kisker, C. (2000) The nucleotide excision repair protein UvrB, a helicase-like enzyme with a catch. *Mutat. Res. 460*, 277–300.
16. Van Houten, B., Illenye, S., Qu, Y., and Farrell, N. (1993) Homodinuclear (Pt,Pt) and Heterodinuclear (Ru,Pt) Metal-Compounds as DNA-Protein Cross-Linking Agents: Potential Suicide DNA Lesions. *Biochemistry 32*, 11794–11801.
17. Myles, G. M., Van Houten, B., and Sancar, A. (1987) Utilization of DNA Photolyase, Pyrimidine Dimer Endonucleases, and Alkali Hydrolysis in the Analysis of Aberrant Abc Excinuclease Incisions

Adjacent to UV-Induced DNA Photoproducts. *Nucleic Acids Res. 15*, 1227–1243.
18. Van Houten, B., Gamper, H., Holbrook, S. R., Hearst, J. E., and Sancar, A. (1986) Action Mechanism of Abc Excision Nuclease on a DNA Substrate Containing a Psoralen Cross-Link at a Defined Position. *Proc. Natl. Acad. Sci. U.S.A. 83*, 8077–8081.
19. Zou, Y., Liu, T. M., Geacintov, N. E., and Van Houten, B. (1995) Interaction of the UvrABC nuclease system with a DNA duplex containing a single stereoisomer of dG-(+)- or dG-(−)-anti-BPDE. *Biochemistry 34*, 13582–13593.
20. Sibghat, U., Sancar, A., and Hearst, J. E. (1990) The repair patch of *E. coli* (A)BC excinuclease. *Nucleic Acids Res. 18*, 5051–5053.
21. Malta, E., Moolenaar, G. F., and Goosen, N. (2006) Base flipping in nucleotide excision repair. *J. Biol. Chem. 281*, 2184–2194.
22. Malta, E., Verhagen, C. P., Moolenaar, G. F., Filippov, D. V., van der Marel, G. A., and Goosen, N. (2008) Functions of base flipping in *E. coli* nucleotide excision repair. *DNA Repair 7*, 1647–1658.
23. Moolenaar, G. F., Schut, M., and Goosen, N. (2005) Binding of the UvrB dimer to non-damaged and damaged DNA: Residues Y92 and Y93 influence the stability of both subunits. *DNA Repair 4*, 699–713.
24. Moolenaar, G. F., Hoglund, L., and Goosen, N. (2001) Clue to damage recognition by UvrB: Residues in the β-hairpin structure prevent binding to non-damaged DNA. *EMBO J. 20*, 6140–6149.
25. Zou, Y., Ma, H., Minko, I. G., Shell, S. M., Yang, Z., Qu, Y., Xu, Y., Geacintov, N. E., and Lloyd, R. S. (2004) DNA damage recognition of mutated forms of UvrB proteins in nucleotide excision repair. *Biochemistry 43*, 4196–4205.
26. Truglio, J. J., Karakas, E., Rhau, B., Wang, H., DellaVecchia, M. J., Van Houten, B., and Kisker, C. (2006) Structural basis for DNA recognition and processing by UvrB. *Nat. Struct. Mol. Biol. 13*, 360–364.
27. Waters, T. R., Eryilmaz, J., Geddes, S., and Barrett, T. E. (2006) Damage detection by the UvrABC pathway: Crystal structure of UvrB bound to fluorescein-adducted DNA. *FEBS Lett. 580*, 6423–6427.
28. Mees, A., Klar, T., Gnau, P., Hennecke, U., Eker, A. P., Carell, T., and Essen, L. O. (2004) Crystal structure of a photolyase bound to a CPD-like DNA lesion after in situ repair. *Science 306*, 1789–1793.
29. Sancar, A., Franklin, K. A., and Sancar, G. B. (1984) *Escherichia coli* DNA photolyase stimulates uvrABC excision nuclease in vitro. *Proc. Natl. Acad. Sci. U.S.A. 81*, 7397–7401.
30. Conney, A. H. (1982) Induction of microsomal enzymes by foreign chemicals and carcinogenesis by polycyclic aromatic hydrocarbons: G. H. A. Clowes Memorial Lecture. *Cancer Res. 42*, 4875–4917.
31. Cheng, S. C., Hilton, B. D., Roman, J. M., and Dipple, A. (1989) DNA adducts from carcinogenic and noncarcinogenic enantiomers of benzo[a]pyrene dihydrodiol epoxide. *Chem. Res. Toxicol. 2*, 334–340.
32. Meehan, T., and Straub, K. (1979) Double-stranded DNA steroselectively binds benzo(a)pyrene diol epoxides. *Nature 277*, 410–412.
33. Jiang, G. H., Skorvaga, M., Croteau, D. L., Van Houten, B., and States, J. C. (2006) Robust incision of benoz[a]pyrene-7,8-dihyrodiol-9,10-epoxide-DNA adducts by a recombinant thermoresistant interspecies combination UvrABC endonuclease system. *Biochemistry 45*, 7834–7843.
34. Eryilmaz, J., Ceschini, S., Ryan, J., Geddes, S., Waters, T. R., and Barrett, T. E. (2006) Structural insights into the cryptic DNA-dependent ATPase activity of UvrB. *J. Mol. Biol. 357*, 62–72.
35. Theis, K., Chen, P. J., Skorvaga, M., Van Houten, B., and Kisker, C. (1999) Crystal structure of UvrB, a DNA helicase adapted for nucleotide excision repair. *EMBO J. 18*, 6899–6907.
36. Min, J. H., and Pavletich, N. P. (2007) Recognition of DNA damage by the Rad4 nucleotide excision repair protein. *Nature 449*, 570–575.
37. Moolenaar, G. F., Franken, K. L., Dijkstra, D. M., Thomas-Oates, J. E., Visse, R., van de Putte, P., and Goosen, N. (1995) The C-terminal region of the UvrB protein of *Escherichia coli* contains an important determinant for UvrC binding to the preincision complex but not the catalytic site for 3′-incision. *J. Biol. Chem. 270*, 30508–30515.
38. Wang, H., DellaVecchia, M. J., Skorvaga, M., Croteau, D. L., Erie, D. A., and Van Houten, B. (2006) UvrB domain 4, an autoinhibitory gate for regulation of DNA binding and ATPase activity. *J. Biol. Chem. 281*, 15227–15237.
39. Cosman, M., de los Santos, C., Fiala, R., Hingerty, B. E., Ibanez, V., Luna, E., Harvey, R., Geacintov, N. E., Broyde, S., and Patel, D. J. (1993) Solution conformation of the (+)-cis-anti-[BP]dG adduct in a DNA duplex: Intercalation of the covalently attached benzo-[a]pyrenyl ring into the helix and displacement of the modified deoxyguanosine. *Biochemistry 32*, 4145–4155.
40. Cosman, M., de los Santos, C., Fiala, R., Hingerty, B. E., Singh, S. B., Ibanez, V., Margulis, L. A., Live, D., Geacintov, N. E., and Broyde, S. (1992) Solution conformation of the major adduct between the carcinogen (+)-anti-benzo[a]pyrene diol epoxide and DNA. *Proc. Natl. Acad. Sci. U.S.A. 89*, 1914–1918.
41. Skorvaga, M., DellaVecchia, M. J., Croteau, D. L., Theis, K., Truglio, J. J., Mandavilli, B. S., Kisker, C., and Van Houten, B. (2004) Identification of residues within UvrB that are important for efficient DNA binding and damage processing. *J. Biol. Chem. 279*, 51574–51580.
42. Case, D. A., Darden, T. A., Cheatham, T. E., III, Simmerling, C. L., Wang, J., Duke, R. E., Luo, R., Merz, K. M., Wang, B., Pearlman, D. A., et al. (2004) AMBER 8 , University of California, San Francisco.
43. Cornell, W. D., Cieplak, P., Bayly, C. I., Gould, I. R., Merz, K. M., Ferguson, D. M., Spellmeyer, D. C., Fox, T., Caldwell, J. W., and Kollman, P. A. (1995) A Second Generation Force Field for the Simulation of Proteins, Nucleic Acids, and Organic Molecules. *J. Am. Chem. Soc. 117*, 5179–5197.
44. Wang, J. M., Cieplak, P., and Kollman, P. A. (2000) How well does a restrained electrostatic potential (RESP) model perform in calculating conformational energies of organic and biological molecules? *J. Comput. Chem. 21*, 1049–1074.
45. Jia, L., Shafirovich, V., Shapiro, R., Geacintov, N. E., and Broyde, S. (2005) Structural and thermodynamic features of spiroiminodihydantoin damaged DNA duplexes. *Biochemistry 44*, 13342–13353.
46. Wang, J. M., Wolf, R. M., Caldwell, J. W., Kollman, P. A., and Case, D. A. (2004) Development and testing of a general amber force field. *J. Comput. Chem. 25*, 1157–1174.
47. Simmerling, C., and Kollman, P. (1996) MOIL-View: A program for visualization of structure and dynamics of biomolecules. Abstracts of Papers of the American Chemical Society , Vol. 211, 92-Comp, American Chemical Society, Washington, DC.
48. Xie, X. M., Geacintov, N. E., and Broyde, S. (1999) Origins of conformational differences between cis and trans DNA adducts derived from enantiomeric anti-benzo[a]pyrene diol epoxides. *Chem. Res. Toxicol. 12*, 597–609.
49. Case, D. A., Pearlman, D. A., Caldwell, J. W., Cheatham, T. E., III, Wang, J., Ross, W. S., Simmerling, C. L., Darden, T. A., Merz, K. M., Stanton, R. V., et al. (2002) AMBER 7 , University of California, San Francisco.
50. DeLano, W. L. (2002) PyMOL , DeLano Scientific, San Carlos, CA.
51. Carell, T., Burgdorf, L. T., Kundu, L. M., and Cichon, M. (2001) The mechanism of action of DNA photolyases. *Curr. Opin. Chem. Biol. 5*, 491–498.
52. Sancar, A. (2003) Structure and function of DNA photolyase and cryptochrome blue-light photoreceptors. *Chem. Rev. 103*, 2203–2237.
53. Malta, E., Moolenaar, G. F., and Goosen, N. (2007) Dynamics of the UvrABC nucleotide excision repair proteins analyzed by fluorescence resonance energy transfer. *Biochemistry 46*, 9080–9088.
54. Karakas, E., Truglio, J. J., Croteau, D., Rhau, B., Wang, L., Van Houten, B., and Kisker, C. (2007) Structure of the C-terminal half of UvrC reveals an RNase H endonuclease domain with an Argonaute-like catalytic triad. *EMBO J. 26*, 613–622.
55. Nakano, T., Morishita, S., Katafuchi, A., Matsubara, M., Horikawa, Y., Terato, H., Salem, A. M., Izumi, S., Pack, S. P., and Makino, K., et al. (2007) Nucleotide excision repair and homologous recombination systems commit differentially to the repair of DNA-protein crosslinks. *Mol. Cell 28*, 147–158.
56. Huffman, J. L., Sundheim, O., and Tainer, J. A. (2005) DNA base damage recognition and removal: New twists and grooves. *Mutat. Res. 577*, 55–76.
57. Parker, J. B., Bianchet, M. A., Krosky, D. J., Friedman, J. I., Amzel, L. M., and Stivers, J. T. (2007) Enzymatic capture of an extrahelical thymine in the search for uracil in DNA. *Nature 449*, 433–437.
58. Mocquet, V., Kropachev, K., Kolbanovskiy, M., Kolbanovskiy, A., Tapias, A., Cai, Y., Broyde, S., Geacintov, N. E., and Egly, J. M. (2007) The human DNA repair factor XPC-HR23B distinguishes stereoisomeric benzo[a]pyrenyl-DNA lesions. *EMBO J. 26*, 2923–2932.
59. Buterin, T., Meyer, C., Giese, B., and Naegeli, H. (2005) DNA quality control by conformational readout on the undamaged strand of the double helix. *Chem. Biol. 12*, 913–922.
60. Scharer, O. D. (2008) A molecular basis for damage recognition in eukaryotic nucleotide excision repair. *ChemBioChem 9*, 21–23.
61. Scrima, A., Konickova, R., Czyzewski, B. K., Kawasaki, Y., Jeffrey, P. D., Groisman, R., Nakatani, Y., Iwai, S., Pavletich, N. P., and Thoma, N. H. (2008) Structural basis of UV DNA-damage recognition by the DDB1-DDB2 complex. *Cell 135*, 1213–1223.